Weierstraß-Institut
für Angewandte Analysis und Stochastik

im Forschungsverbund Berlin e.V.

Preprint ISSN 0946 – 8633

Kinetic flux-vector splitting schemes for the hyperbolic heat conduction

Wolfgang Dreyer, Shamsul Qamar

submitted: 27th August 2003

Weierstrass Institute
for Applied Analysis
and Stochastics
Mohrenstrasse 39
10117 Berlin
Germany
E-Mail: dreyer@wias-berlin.de
qamar@wias-berlin.de

No. 861
Berlin 2003

2000 *Mathematics Subject Classification.* 65M99, 76Y05, 80A99, 76M12, 35L15.

Key words and phrases. Heat transfer, hyperbolic moment system, initial and boundary value problems, Bose-gas, phonons, high order accuracy.

Edited by
Weierstraß-Institut für Angewandte Analysis und Stochastik (WIAS)
Mohrenstraße 39
D — 10117 Berlin
Germany

Fax: + 49 30 2044975
E-Mail: preprint@wias-berlin.de
World Wide Web: http://www.wias-berlin.de/

Abstract

A kinetic solver is developed for the initial and boundary value problems (IBVP) of the symmetric hyperbolic moment system. This nonlinear system of equations is related to the heat conduction in solids at low temperatures. The system consists of a conservation equation for the energy density e and a balance equation for the heat flux Q^i, where e and Q^i are the four basic fields of the theory. We use kinetic flux vector splitting (KFVS) scheme to solve these equations in one and two space dimensions. The flux vectors of the equations are splitted on the basis of the local equilibrium distribution of phonons. The resulting computational procedure is efficient and straightforward to implement. The second order accuracy of the scheme is acheived by using MUSCL-type reconstruction and min-mod nonlinear limitters. The solutions exhibit second order accuracy, and satisfactory resolution of gradients with no spurious oscillations. The secheme is extended to the two-dimensional case in a usual dimensionally split manner. In order to prescribe the boundary data we need the knowledge of the e and Q^i. However, in experiments only one of the quantities can be controlled at the boundary. This problem is removed by using a continuity condition. It turned out that after some short time energy and heat flux are related to each other according to Rankine Hugoniot jump relations. To illustrate the performance of the KFVS scheme, we perform several one- and two-dimensional test computations. For the comparison of our results we use high order central schemes. The present study demonstrates that this kinetic method is effective in handling such problems.

1 Introduction

Heat conduction processes are usually described by a parabolic system. It results from a diffusion law, where the heat flux is proportional to the temperature gradient. That constitutive law implies the paradox of heat conduction whereupon heat may traverse a body with infinite speed. This fact is not acceptable from physical point of view. In most technical process, in particular at room temperature, those modes that propagate with infinite speed suffer a considerable damping and are thus not observable. However, there are cases where either the damping of heat pulses is quite low or where its travel distance is so small that the transit time is an observable quantity. In those cases the parabolic system has to be replaced by physically justified hyperbolic system of heat conduction. A comprehensive study of many phenomena which appear in the temperature range between $5^o\,K$ and $20^o\,K$ is described in the papers of Dreyer, Kunik and Struchtrup [2, 5]. In that range heat conduction of crystalline solids must be considered as the motion of phonons which may interact with the lattice impurities and with each other. The articles [2, 5] report

on special circumstances that are met in a quite pure crystal at not too low temperature. Here the state of crystal is sufficiently described by four thermodynamic fields as the basic variables. These are the energy density e, or the temperature T, and the heat flux $\mathbf{Q} = (Q^i)_{i=1,2,3}$. The resulting system of field equations is of the symetric hyperbolic type.

In this paper we consider this system in one and two space dimensions and solve it for initial and boundary value problems (IBVP). This nonlinear system consist of a conservation equation for the energy density e and a balance equation for the heat flux Q^i, and it is derived by averaging of the BPE. The closure problem is solved by the *Maximum Entropy Principle* [4]. The IBVP that uses exclusively prescirbed boundary data for the energy density e is solved by a kinetic approach. The kinetic representation of the IBVP reveal a peculiar phenomenon. The contributions to the solution are from intial data at the right of the wall, as well as the fields at the wall e_w and Q_w. However, only one of these quantities can be controlled in an experiment. To overcome this problem we use a continuity condition, see [2]. It turns out that after short time energy and heat flux are related to each other according to the Rankine Hugoniot jump relations given in [2, 4].

Flux splitting is a technique for achieving upwinding bias in numerical flux function, which is a natural consequence of regarding a fluid as an ensemble of particles. Since particles can move forward or backward, this automatically splits the fluxes of mass, momentum and energy into forward and backward fluxes through the cell interface, i.e.,

$$F_{i+\frac{1}{2}} = F^+(W_i) + F^-(W_{i+1}),$$

where W_i in our case represents the energy density and heat flux inside the cell i. Alhough kineitc flux vector splitting (KFVS) scheme is based on the free particle transport, an artificial collision term has been implicitly added in the projection stage. For example at the end of each time step, a phonon distribution function f_N inside each cell is re-initiated, which is equivalent to perform particle collisions instantaneously to make the transition from non-equilibrium state, i.e. free-flight f, to equilibrium state f_N inside each cell. The dynamical effect from the two numerical stages (i.e. free-flight and projection) in the KFVS scheme is qualitatively described in the Figure 1, where the free transport in the evolution stage evolves the system away from the equilibrium solution (f becomes more and more different from a equilibrium distribution of phonons), the projection stage drives the system towards the equilibrium solution (the instantaneous preparation of equilibrium states), in case of Euler equations see Xu [15].

In the KFVS scheme we start with a cell averaged initial data of the conservative variables e, Q^i, and get back the cell averaged values of the conservative variables at the next time step. In the two-dimensional case the flux splitting is done in a usual dimensionally split manner, that is, the formulae for the fluxes can be used along each coordinate direction. In order to get second order accuracy we use the MUSCL-type reconstruction in both one and two-dimensional cases.

In 1929, Peierls [13] proposed his celebrated theoretical model based on the Boltzmann equation. According to him the lattice vibrations responsible for the heat transport can be described as an interacting gas of phonons. The Boltzmann-Peierls approach is one of the milestones of the theory of thermal transport in solids, especially at very low temperatures.

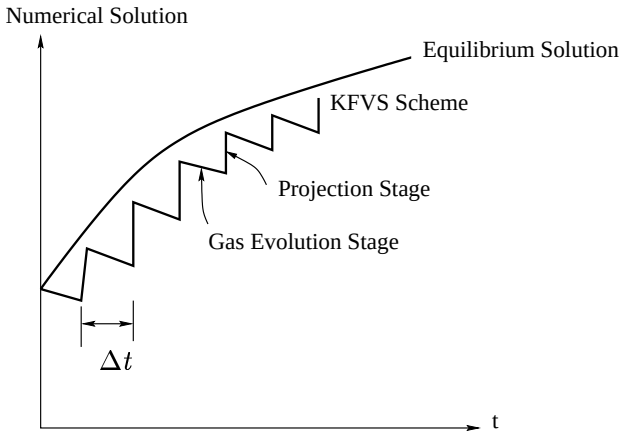

Figure 1: KFVS solution vs moment sytem solution.

It is important to mention that Fourier theory of heat flow fails to describe heat conduction processes at low temperatures, see for example Dreyer and Struchtrup [5] and references therein.

It is important to mention that the ideas used in this paper were also utilized to obtain the kinetic solution of the ultra-relativistic Euler equations, see Kunik, Qamar and Warnecke [7, 8, 10].

This paper consist of seven sections. In Section 2, we recall the three-dimensional BPE and its hyperbolic moment system [3, 5, 9]. In Section 3, we give the kinetic schemes for the hyperbolic moment system in three space dimensions. We reduce the three-dimensional moment integrals to two-fold surface integrals by using polar coordinates. Using special coordinates, we futher reduce the already reduced moment integrals in one and two space dimensions. In Section 4, we use the KFVS scheme in order to solve the one-dimensional hyperbolic moment system. We extend the scheme to second order by using MUSCL-type reconstruction. We also extend the scheme to account for the boundary conditions. In Section 5, we solve the two-dimensional hyperbolic moment system. We also extend the scheme to second order by using MUSCl-type reconstruction. In Section 6 we give some numerical test computations in one and two space dimensions. For the comparison of our results from KFVS scheme we use high order central schemes [6, 11, 12]. In Section 7, we give the conclusions about the results.

2 BPE and its Hyperbolic Moment System

The Boltzmann-Peierls equation is a kinetic equation for the phase density of phonons. This equation describes the evolution of the phase density $f(t, \mathbf{x}, \mathbf{k})$, where $f(t, \mathbf{x}, \mathbf{k})d^3xd^3k$ is interpreted as the number of phonons at time t in an infinitesimally small phase cell element d^3xd^3k centered at $(\mathbf{x}, \mathbf{k})$. Here $\hbar\mathbf{k}$ denote the momentum, $\mathbf{k}$ the phonon wave vector and $\hbar$ is Planck's constant, see [13, 5] for further details. The microscopically three dimensional

Boltzmann-Peierls equation (BPE) can be written as

$$\frac{\partial f}{\partial t} + \frac{\partial \omega}{\partial k_k}\frac{\partial f}{\partial x^i} = \zeta(f)\,, \tag{2.1}$$

where ω is the phonon frequency, t is time, and ζ is the collision operator which will be defined below. In a real crystal there are three phonon modes and thus there are three phase densities corresponding to two transversal modes and one longitudinal mode. In [5] it is described that for simplicity one can replace the actual crystal by a so called *Debye solid*, which is characterized by a single mode only. In addition the assumed dispersion relation between the phonon frequency ω and the wave vector $\mathbf{k}$ is given by

$$\omega = c\,|\mathbf{k}|\,. \tag{2.2}$$

Here the Debye velocity c is related to mean of the two transveral and longitudinal sound speeds of the actual crystal. Thus the BPE is given by

$$\frac{\partial f}{\partial t} + c\sum_{i=1}^{3}\frac{k^i}{|\mathbf{k}|}\frac{\partial f}{\partial x^i} = \zeta(f)\,. \tag{2.3}$$

The moments of the phase density f reflect the kinetic processes on the scale of continuum physics. The most important moments are

$$e(t,\mathbf{x}) = \hbar c\int_{-\infty}^{\infty}|\mathbf{k}|\,f(t,\mathbf{x},\mathbf{k})\,d^3k\,, \tag{2.4}$$

$$Q^i(t,\mathbf{x}) = \hbar c^2\int_{-\infty}^{\infty}k^i f(t,\mathbf{x},\mathbf{k})\,d^3k\,, \tag{2.5}$$

$$N^{ij}(t,\mathbf{x}) = \hbar c\int_{-\infty}^{\infty}\frac{k^ik^j}{|\mathbf{k}|}f(t,\mathbf{x},\mathbf{k})\,d^3k\,,\quad i,j=1,2,3\,. \tag{2.6}$$

The fields e, $\mathbf{Q}=(Q^1,Q^2,Q^3)$ and the Matrix $\mathbf{N}=(N^{ij})$ are the energy density, heat flux and momentum flux, respectively. Phonons are classified as Bose particles [13, 5], and the corresponding entropy density-entropy flux pair (h,φ) is given by

$$h(f) := y\int_{\mathbb{R}^3}\left[\left(1+\frac{f}{y}\right)\ln\left(1+\frac{f}{y}\right)-\frac{f}{y}\ln\left(\frac{f}{y}\right)\right]d^3k\,, \tag{2.7}$$

$$\varphi^i(f) := yc\int_{\mathbb{R}^3}\frac{k^i}{|\mathbf{k}|}\left[\left(1+\frac{f}{y}\right)\ln\left(1+\frac{f}{y}\right)-\frac{f}{y}\ln\left(\frac{f}{y}\right)\right]d^3k\,, \tag{2.8}$$

where $y=\frac{3}{8\pi^3}$, see [5] .

In contrast to the ordinary gas atoms, the phonons may interact by two different collision processes, called R- and N-processes. R-processes include interactions of phonons with

lattice impurities which destroy the periodicity of the crystal, while N-processes can be interpreted as phonon-phonon interactions which are due to the deviations from harmonicity of the crystal forces. N-processes conserve both, energy and momentum, while R-processes only conserve energy. The Callaway approximation of the collision operator [1, 5] is a suitable simplification of the actual interaction processes. The Callaway collision operator is written as the sum of two relaxation operators modelling the R- and N-processes seperately. We write

$$\zeta(f) = \zeta_R(f) + \zeta_N(f)\,, \qquad \zeta_\alpha = \frac{1}{\tau_\alpha}\left(P_\alpha f - f\right)\,, \quad \alpha \in \{R, N\}\,. \tag{2.9}$$

The positive constants τ_R and τ_N are the relaxation times, while P_R and P_N are two nonlinear projectors. Here $P_R f$ and $P_N f$ represent the phase densities in the limiting case when the relaxation time tends to zero. Explicitly, we define $P_R f$ and $P_N f$ as the solutions of two optimization problems, namely

$$h(P_R f) = \max_{f'}\left\{h(f) \;:\; e(f') = e(f)\right\}\,, \tag{2.10}$$

$$h(P_N f) = \max_{f'}\left\{h(f) \;:\; e(f') = e(f),\, \mathbf{Q}(f') = \mathbf{Q}(f)\right\}\,, \tag{2.11}$$

where $e(f)$, $\mathbf{Q}(f)$ are given by (2.4), (2.5). The maximization problems can be solved by means of Lagrange multipliers Λ_R^0 and Λ_N^0, Λ_N^1, Λ_N^2, Λ_N^3. Therefore we get

$$P_R f(\mathbf{k}) = \frac{y}{-1 + \exp(\Sigma_R)}\,, \qquad P_N f(\mathbf{k}) = \frac{y}{-1 + \exp(\Sigma_N)}\,, \tag{2.12}$$

where

$$\Sigma_R(t, \mathbf{x}, \mathbf{k}) = \hbar c\,|\mathbf{k}|\,\Lambda_R^0\,, \tag{2.13}$$

$$\Sigma_N(t, \mathbf{x}, \mathbf{k}) = \hbar c\,|\mathbf{k}|\,\Lambda_N^0(t, \mathbf{x}) + \hbar\, k^i\,\Lambda_N^i(t, \mathbf{x})\,. \tag{2.14}$$

From (2.10) and (2.11) the Lagrange multipliers can be calculated explicitly. They are given by, see [2], [3],

$$\Lambda_R^0 = \left(\frac{10\hbar^3 c^3}{\pi^2} e\right)^{-\frac{1}{4}}\,, \quad \Lambda_N^0 = \gamma \frac{\left(\frac{F}{e}\right)^{\frac{1}{4}}}{(4-F)^{\frac{3}{4}}}\,, \quad \Lambda_R^i = -\frac{\gamma}{4}\frac{\left(\frac{F}{e}\right)^{\frac{5}{4}}}{(4-F)^{\frac{3}{4}}} Q^i\,, \tag{2.15}$$

$$F = \frac{6}{1 + \sqrt{1 - \frac{3}{4}\left(\frac{|\mathbf{Q}|}{ce}\right)^2}}\,, \quad \gamma = \left(\frac{4\pi^5 y}{45\hbar^3 c^3}\right)^{\frac{1}{4}}\,. \tag{2.16}$$

When the thermodynamic state is described by four fields e and Q^i only, then we can derive the following balance equations from the Boltzmann-Peierls equation (2.3) and the maximum entropy principle, see [2],

$$\begin{aligned} \frac{\partial e}{\partial t} + \frac{\partial Q^i}{\partial x^i} &= 0\,, \\ \frac{\partial Q^i}{\partial t} + \frac{\partial\left(c^2 N^{ij}\right)}{\partial x^j} &= -\frac{1}{\tau_R} Q^i\,, \quad i, j = 1, 2, 3, \\ N^{ij} &= \frac{1}{3} e\,\delta^{ij} + \frac{1}{2} e(3\chi - 1)\left(\frac{Q^i Q^j}{|\mathbf{Q}|^2} - \frac{1}{3}\delta^{ij}\right)\,, \end{aligned} \tag{2.17}$$

where χ is the so called Eddington-factor:

$$\chi = \frac{5}{3} - \frac{4}{3}\sqrt{1 - \frac{3}{4}\left(\frac{|\mathbf{Q}|}{ce}\right)^2}. \tag{2.18}$$

Note that in above equations (2.17) the τ_N term do not appear on the right hand side, therefore the applicability of these equations is restricted to the relaxation limit $\tau_N \to 0$.

We can rewrite (2.17) as

$$\frac{\partial W}{\partial t} + \sum_{i=1}^{3} \frac{\partial F^i(W)}{\partial x^i} = S(W)\,, \tag{2.19}$$

where

$$W = \begin{pmatrix} e \\ Q^1 \\ Q^2 \\ Q^3 \end{pmatrix}\,, \quad F^i(W) = \begin{pmatrix} Q^i \\ c^2 N^{1i} \\ c^2 N^{2i} \\ c^2 N^{3i} \end{pmatrix}\,, \quad S(W) = -\frac{1}{\tau_R}\begin{pmatrix} 0 \\ Q^1 \\ Q^2 \\ Q^3 \end{pmatrix}\,, \tag{2.20}$$

3 Moments of the Linear Transport Equation

The linear transport equation (2.3) without collision term is given by

$$\begin{aligned} &\frac{\partial f}{\partial t} + c\sum_{i=1}^{3} \frac{k^i}{|\mathbf{k}|}\frac{\partial f}{\partial x^i} = 0\,, \\ &\text{with I.D. } f(t_n, \mathbf{x}, \mathbf{k}) = f_n(\mathbf{x}, \mathbf{k})\,. \end{aligned} \tag{3.1}$$

The exact solution of(3.1) for $t_n \le \tau < t_{n+1} = t_n + \Delta t$ is

$$f(t_n + \tau, \mathbf{x}, \mathbf{q}) = f_n(x - \tau\frac{\mathbf{k}}{|\mathbf{k}|}, \mathbf{k})\,. \tag{3.2}$$

Using (3.2) in the moment integrals (2.4), (2.5) and (2.6) we get

$$\begin{aligned} e(t_n + \tau, \mathbf{x}) &= \int_{\mathbb{R}^3} |\mathbf{k}|\, f_n(\mathbf{x} - \tau\frac{\mathbf{k}}{|\mathbf{k}|}, \mathbf{k}) d^3k\,, \\ Q^i(t_n + \tau, \mathbf{x}) &= \int_{\mathbb{R}^3} k^i f_n(\mathbf{x} - \tau\frac{\mathbf{k}}{|\mathbf{k}|}, \mathbf{k}) d^3k\,, \\ N^{ij}(t_n + \tau, \mathbf{x}) &= \int_{\mathbb{R}^3} \frac{k^i k^j}{|\mathbf{k}|} f_n(\mathbf{x} - \tau\frac{\mathbf{k}}{|\mathbf{k}|}, \mathbf{k}) d^3k\,, \end{aligned} \tag{3.3}$$

where f_n is phonon initial phase density at time t_n

$$f_n(\mathbf{y}, \mathbf{q}) = P_N f(e(t_n, \mathbf{y}), \mathbf{Q}(t_n, \mathbf{y}), \mathbf{k})\,. \tag{3.4}$$

Now we can simplify the volume integrals (3.3) for the free flight moments. We can see in (3.4) that the fields $e(t,\mathbf{y})$ and $\mathbf{Q}(t,\mathbf{y})$ are not depending on $|\mathbf{k}|$ but only on the unit vector $\mathbf{n} = (n^1, n^2, n^3)^T = \frac{\mathbf{k}}{|\mathbf{k}|}$. This fact enables us to reduce the three-fold volume integrals to the two-fold surface integrals by applying polar coordinates, see [2, 7].

The phonons phase density $P_N f$ depends on the wave vector $\mathbf{k} \in \mathbb{R}^3$, therefore we can calculate the reduced phonons phase density according to the radial integration in polar-coordinates:

$$\Psi_N(\mathbf{y},\mathbf{n}) = \hbar c \int_0^\infty |\mathbf{k}|^3 \, P_N f(t_n, \mathbf{y}, |\mathbf{k}|\,\mathbf{n})\, d|\mathbf{k}| \,. \tag{3.5}$$

Using the abbreviations

$$\Psi_N = \frac{3}{4\pi} \frac{e(4-F)^3}{F\left(1 - \frac{F\, n^i Q^i}{4\, c\, e}\right)^4}\,, \qquad F = \frac{6}{1 + \sqrt{1 - \frac{3}{4}\left(\frac{|\mathbf{Q}|}{c\, e}\right)^2}}, \tag{3.6}$$

we have

$$\begin{aligned} e(t_n + \tau, \mathbf{x}) &= \oint_{\partial B(0,1)} \Psi_N(\mathbf{x} - \tau\mathbf{n}, \mathbf{n})\, dS(\mathbf{n})\,, \\ Q^i(t_n + \tau, \mathbf{x}) &= c \oint_{\partial B(0,1)} n^i\, \Psi_N(\mathbf{x} - \tau\mathbf{n}, \mathbf{n})\, dS(\mathbf{n})\,, \\ N^{ij}(t_n + \tau, \mathbf{x}) &= \oint_{\partial B(0,1)} n^i\, n^j\, \Psi_N(\mathbf{x} - \tau\mathbf{n}, \mathbf{n})\, dS(\mathbf{n})\,. \end{aligned} \tag{3.7}$$

Here $\mathbf{n} = \frac{\mathbf{k}}{|\mathbf{k}|}$ is the unit vector in direction of $\mathbf{k}$ and $B(\mathbf{x}_0, r)$ is the ball with radius r and center $\mathbf{x}_0$. Its boundary is the sphere $\partial B(\mathbf{x}_0, r)$.

Furthermore if we introduce instead of the unit vector $\mathbf{n}$ the new variables $-1 \le \xi \le 1$ and $-\pi \leqq \varphi \leqq \pi$ by

$$n^1 = \xi\,, \qquad n^2 = \sqrt{1-\xi^2}\sin\varphi\,, \qquad n^3 = \sqrt{1-\xi^2}\cos\varphi\,, \tag{3.8}$$

then the simplified free-flight moments integrals for the one- and two-dimensional cases are given below, see [2, 7].

One dimensional moment integrals

Here we only consider solutions which depend on t and $x = x^1$ and satisfy $e = e(t,x)$, $\mathbf{Q} = (Q(t,x), 0, 0)$. In this case the quantities e, Q in the free flight phase density are not depending on the variable φ. This fact enables us to carry out the integration with respect to φ directly. Thus the two-fold surface integrals reduces to simple $\xi-$integrals. For

abbreviation we introduce

$$\Psi_N = \frac{3}{2}\frac{e(4-F)^3}{F\left(1-\frac{F\,\xi\,Q}{4\,c\,e}\right)^4}\,, \quad F = \frac{6}{1+\sqrt{1-\frac{3}{4}\left(\frac{|Q|}{c\,e}\right)^2}}, \tag{3.9}$$

then the reduced integrals for the moments can be written as

$$W(t_n+\tau,x) = \begin{pmatrix} e(t_n+\tau,x) \\ Q(t_n+\tau,x) \end{pmatrix} = \int_{-1}^{1} \begin{pmatrix} \Psi_N(x-\tau\xi,\xi) \\ c\xi\,\Psi_n(x-\tau\xi,\xi) \end{pmatrix} d\xi, \tag{3.10}$$

$$F(t_n+\tau,x) = \begin{pmatrix} Q(t_n+\tau,x) \\ N(t_n+\tau,x) \end{pmatrix} = \int_{-1}^{1} \begin{pmatrix} c\xi\,\Phi(x-\tau\xi,\xi) \\ \xi^2\,\Psi(x-\tau\xi,\xi) \end{pmatrix} d\xi\,. \tag{3.11}$$

Two Dimensional moment integrals

In this case we consider the solutions which depend on t, $x = x^1$ and $y = x^2$ and satisfy $e = e(t,x,y)$, $\mathbf{Q} = (Q^1(t,x,y), Q^2(t,x,y), 0)$. Instead of the unit vector $\mathbf{n}$, we use again the new variables in (3.8). Then the moment integrals take again a simplier form, namely

$$W(t_n+\tau,x,y) = \begin{pmatrix} e(t_n+\tau,x,y) \\ Q^1(t_n+\tau,x,y) \\ Q^2(t_n+\tau,x,y) \end{pmatrix} = \int_{-\pi}^{\pi}\int_{-1}^{1} \begin{pmatrix} \Psi_N(\mathbf{y},n^1,n^2) \\ cn^1\,\Psi_N(\mathbf{y},n^1,n^2) \\ cn^2\,\Psi_N(\mathbf{y},n^1,n^2) \end{pmatrix} d\xi d\varphi\,, \tag{3.12}$$

$$F(t_n+\tau,x,y) = \begin{pmatrix} Q^1(t_n+\tau,x,y) \\ N^{11}(t_n+\tau,x,y) \\ N^{12}(t_n+\tau,x,y) \end{pmatrix} = \int_{-\pi}^{\pi}\int_{-1}^{1} \begin{pmatrix} cn^1\,\Psi_N(\mathbf{y},n^1,n^2) \\ (n^1)^2\,\Psi_N(\mathbf{y},n^1,n^2) \\ n^1n^2\,\Psi_N(\mathbf{y},n^1,n^2) \end{pmatrix} d\xi d\varphi\,, \tag{3.13}$$

$$G(t_n+\tau,x,x,y) = \begin{pmatrix} Q^2(t_n+\tau,x,y) \\ N^{21}(t_n+\tau,x,y) \\ N^{22}(t_n+\tau,x,y) \end{pmatrix} = \int_{-\pi}^{\pi}\int_{-1}^{1} \begin{pmatrix} n^2\,\Psi_N(\mathbf{y},n^1,n^2) \\ n^1n^2\,\Psi_N(\mathbf{y},n^1,n^2) \\ (n^2)^2\,\Psi_N(\mathbf{y},n^1,n^2) \end{pmatrix} d\xi d\varphi\,,$$

where $\mathbf{y} = x-\tau n^1, y-\tau n^2$ and Ψ_N is given by (3.6). The above one- and two-dimensional free-flight moments integrals will be used in order to derive kinetic flux splitting (KFVS) schemes for the one- and two-dimensional hyperbolic heat conducton equations.

4 One-Dimensional KFVS Scheme

Here we want to solve the one dimensional moment system

$$\frac{\partial W}{\partial t} + \frac{\partial F(W)}{\partial x} = S(W)\,, \tag{4.1}$$

where

$$W = \begin{pmatrix} e \\ Q \end{pmatrix}, \quad F(W) = \begin{pmatrix} Q \\ c^2 N \end{pmatrix}, \quad S(W) = -\frac{1}{\tau_R}\begin{pmatrix} 0 \\ Q \end{pmatrix}. \tag{4.2}$$

We start with a piecewise constant initial data $\overline{W}_i^n$ at time t_n over the cells $[x_{i-\frac{1}{2}}, x_{i+\frac{1}{2}}]$ of a given mesh size $\Delta x = x_{i+\frac{1}{2}} - x_{i-\frac{1}{2}}$. We have to compute $\overline{W}_i^{n+1}$ at time $t_{n+1} = t_n + \Delta t$ over the same cells. We take the natural CFL condition $\Delta t = \frac{\Delta x}{2}$ in order to ensure that neighbouring waves will not interact. The left hand side of (4.1) can be approximated by a first-order upwind conservative scheme. For the nonlinear relaxation term on the left hand side, a standered centered approximation technique is used, see . Our scheme thus reads

$$\overline{W}_i^{n+1} = \overline{W}_i^n - \lambda\left[F_{i+\frac{1}{2}}^n - F_{i-\frac{1}{2}}^n\right] + \Delta t \overline{S}_i^n, \tag{4.3}$$

where $\lambda = \frac{\Delta t}{\Delta x}$ and $F_{i+\frac{1}{2}}^n$ represent the fluxes across the cell interface. From (3.11) we have for $\eta_\alpha = (c\xi, \xi^2)^T$

$$F_{i+\frac{1}{2}}^n = \frac{1}{\Delta t}\int_{t_n}^{t_{n+1}} F(\tau, x_{i+\frac{1}{2}})\, d\tau = \frac{1}{\Delta t}\int_{t_n}^{t_{n+1}}\int_{-1}^{1} \eta_\alpha \Psi_N(x_{i+\frac{1}{2}} - \tau\xi, \xi)\, d\xi\, d\tau\,. \tag{4.4}$$

The CFL condition states that ξ-integration is limited to ξ such that $|\xi|\tau \le \Delta x$. This means that $x_{i\pm\frac{1}{2}} - \xi\tau$ remains in a neighbour cell to $x_{i\pm\frac{1}{2}}$. This implies that the field variables e, Q in the splitted flux integrals will not depend on the $\xi-$integration, therefore equation (4.4) gives

$$\begin{aligned}\frac{1}{\Delta t}\int_{t_n}^{t_{n+1}} F(\tau, x_{i+\frac{1}{2}})\, d\tau &= \int_0^1 \Psi_N(x_i, \xi)\, d\xi + \int_{-1}^0 \Psi_N(x_{i+1}, \xi)\, d\xi \\ &= F_i^+ + F_{i+1}^-\,,\end{aligned} \tag{4.5}$$

where $F_i^\pm = \begin{pmatrix} Q_i^\pm \\ c^2 N_i^\pm \end{pmatrix}$ for each cell I_i, and

$$Q_i^\pm = \frac{4\,c^3\,e_i^3\left[-4 + F_i\right]^3\left[\mp 12\,c\,e_i + F_i\,Q_i\right]}{F_i\left[4\,c\,e_i \mp F_i\,Q_i\right]^3}, \quad N_i^\pm = \frac{32\,c^3\,e_i^4\left[4 - F_i\right]^3}{F_i\left[4\,c\,e_i \mp F_i\,Q_i\right]^3}. \tag{4.6}$$

We finally get the following upwind KFVS scheme

$$\overline{W}_i^{n+1} = \overline{W}_i^n - \lambda\left[F_i^+ + F_{i+1}^- - F_{i-1}^+ - F_i^-\right] + \Delta t \overline{S}_i^n\,. \tag{4.7}$$

4.1 Second Order Extension of the Scheme in 1D

In order to get the second order accuracy we have the following three steps.

(I): **Data Reconstruction.** Starting with a piecewise-constant solution in time and space, $\sum \overline{W}_i^n \chi_i(x)$, one reconstruct a piecewise linear (MUSCL-type) approximation in space, namely

$$W^n(x) = \sum \left[\overline{W}_i^n + W_i^x \frac{(x - x_i)}{\Delta x} \right] \chi_i(x) \, . \tag{4.8}$$

Here, $\chi_i(x)$ is the characteristic function of the cell, $I_i := \{\xi \mid |\xi - x_i| \leq \frac{\Delta x}{2}\}$, centered arround $x_i = i\Delta x$, and W_i^x abbreviates a first-order discrete slopes.

The extreme points $x = 0$ and $x = \Delta x$, in local coordinates correspond to the intercell boundaries in general coordinates $x_{i-\frac{1}{2}}$ and $x_{i+\frac{1}{2}}$, respectively, see Figure 2. The values W_i at the extreme points are

$$W_i^L = \overline{W}_i^n - \frac{1}{2} W_i^x \, , \quad W_i^R = \overline{W}_i^n + \frac{1}{2} W_i^x \, , \tag{4.9}$$

and are usually called *boundary extrapolated values.*

A possible computation of these slopes, which results in an overall nonoscillatory schemes (consult [14]), is given by family of *discrete derivatives* parameterized with $1 \leq \theta \leq 2$, i.e., for any grid function $\{W_i\}$ we set

$$W_i^x = MM\theta\{W_{i-1}, W_i, W_{i+1}\} = MM\left(\theta \Delta W_{i+\frac{1}{2}}, \frac{\theta}{2}(\Delta W_{i-\frac{1}{2}} + \Delta W_{i+\frac{1}{2}}), \theta \Delta W_{i-\frac{1}{2}}\right) \, .$$

Here, Δ denotes the central differencing, $\Delta W_{i+\frac{1}{2}} = W_{i+1} - W_i$, and MM denotes the min-mod nonlinear limiter

$$MM\{x_1, x_2, ...\} = \begin{cases} \min_i\{x_i\} & \text{if } x_i > 0 \quad \forall i \, , \\ \max_i\{x_i\} & \text{if } x_i < 0 \quad \forall i \, , \\ 0 & \text{otherwise} \, . \end{cases} \tag{4.10}$$

This interpolant, (4.8), is then evolved exactly in time and projected on the cell-averages at the next time step.

(II): **Evolution.** For each cell I_i, the boundary extrapolated values W_i^L, W_i^R in (4.9) are evolved for a time $\frac{1}{2}\Delta t$ by

$$\begin{aligned} \hat{W}_i^L &= W_i^L + \frac{1}{2}\frac{\Delta t}{\Delta x}\left[F(W_i^L) - F(W_i^R)\right] + \frac{\Delta t}{2}\overline{S}_i^n \, , \\ \hat{W}_i^R &= W_i^R + \frac{1}{2}\frac{\Delta t}{\Delta x}\left[F(W_i^L) - F(W_i^R)\right] + \frac{\Delta t}{2}\overline{S}_i^n \, . \end{aligned} \tag{4.11}$$

In order to calculate the source term at half time step we need

$$\overline{W}_i^{n+\frac{1}{2}} = \overline{W}_i^n + \frac{1}{2}\frac{\Delta t}{\Delta x}\left[F(W_{i+1}^n) - F(W_i^n)\right] + \frac{\Delta t}{2}\overline{S}_i^n \, , \tag{4.12}$$

where the force F is given by $(4.2)_2$. Note that this evolution step is entirely contained in each cell I_i, as the intercell fluxes are evaluated at the boundary extrapolated values of each cell. At each intercell position $i + \frac{1}{2}$ there are two fluxes, namely W_i^R and W_{i+1}^L, which are in general distinct. This does not really affect the *conservative* character of the overall method, as this step is only an intermediate step [14].

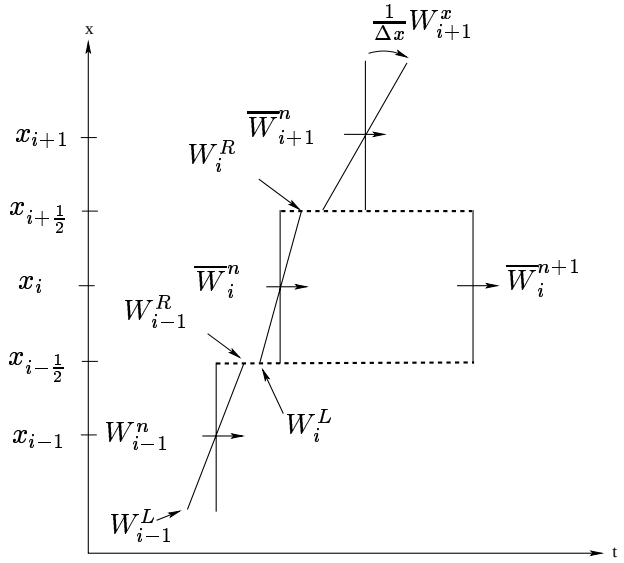

Figure 2: Second Order Reconstruction

(III): Finally we use the conservative formula (4.7) in order to get the conservative variables at next time step

$$\overline{W}_i^{n+1} = \overline{W}_i^n - \frac{\Delta t}{\Delta x}\left[F_{i+\frac{1}{2}}^{n+\frac{1}{2}} - F_{i-\frac{1}{2}}^{n+\frac{1}{2}}\right] + \Delta t\,\overline{S}_i^{n+\frac{1}{2}}\,, \tag{4.13}$$

where $F_{i+\frac{1}{2}}^{n+\frac{1}{2}} = F^+(\hat{W}_i^R) + F^-(\hat{W}_{i+1}^L)$ and $\overline{S}_i^{n+\frac{1}{2}} = S\left(\overline{W}_i^{n+\frac{1}{2}}\right)$.

4.2 Application of Boundary Conditions

Since we are using a conservative scheme, therefore the application of the boundary conditions is not complicated. For the illustration of the boundary conditions we consider half space. We will discuss the boundary conditions only at the left boundary $x = 0$, however the procedure is similar for the other boundary and in multi-dimensional case. We consider the boundary $x = 0$ as a cell interface. We name the moments at the auxiliary cell I_A by e_A^n and on Q_A^n at the left of the boundary $x = 0$ at time t_n. We denote the values of the moments at the wall $x = 0$ by e_w^n and Q_w^n. Once we have the values of the moments at the auxiliary elements, we can calculate the equilibrium phase density at that element. We have the conditions

$$e_w(t_n) = e_A^+(t_n) + e_1^-(t_n)\,, \qquad Q_w(t_n) = Q_A^+(t_n) + Q_1^-(t_n)\,, \tag{4.14}$$

where $e^\pm$ can be obtained in similar way as $Q^\pm$ in (4.6) for a particular element. The fields e_1^n and Q_1^n on the right-hand side of the wall are known from the initial data. We have the following boundary conditions.

Reflecting Boundary Conditions

In this case we need the heat flux at the wall to be zero. Thus we take $e_A^n = e_1^n$ and $Q_A^n = -Q_1^n$, which is equivalent to $\psi_A(t_n, \xi_m) = \Theta_N \psi(e_1^n, |Q_1^n|, -\xi_m)$.

Outflow Boundary Conditions

In this case we need the same values on both sides of the wall. Thus we take $e_A^n = e_1^n$ and $Q_A^n = Q_1^n$, which is equivalent to $\psi_A(t_n, \xi_m) = \Theta_N \psi(e_1^n, |Q_1^n|, \xi_m)$.

Inflow Boundary Conditions

In this case if we are given the values of e_w^n and Q_w^n at the wall then we can use the equations (4.14) in order to find e_A^n and Q_A^n. However, in experimental point of view e_w^n and Q_w^n can not be given simultaneously. Either the energy density e_W^n is controlled at the wall, or the wall is equipped with a procedure of Joule's heat and thus the heat flux is prescribed. Here we consider the case that e_w^n is given from the experiment but not Q_w^n. It turns out that we require the continuity condition $e_A^n = e_w^n$ at each time step t_n. Let us define

$$a^n = \frac{F_A^n Q_A^n}{4\, c\, e_A^n}\,, \qquad f(a^n) = \frac{1}{2}\,\frac{(a^n)^2 \mp 3a^n + 3}{(a^n)^2 + 3}(1 \pm a)^3\,,$$

then $(4.14)_1$ with $e_A^n = e_w^n$ gives

$$e_w^n = e_A^n f(a^n) + e_1^-(t_n)\,,$$

which implies

$$1 - f(a^n) = \frac{e_1^-(t_n)}{e_w^n}\,. \tag{4.15}$$

We know the right-hand side of this equation. Also f(a) is monotonically increasing with $f(-1) = 0$ and $f(1) = 1$, therefore the solution of the above equation only exist whenever the right-hand side is out of the range $[0, 1]$. We use Newton method to solve this equation for the unknown a^n. Finally we determine the auxiliary field Q_A^n according to

$$Q_A^n = \frac{4a^n}{(a^n)^2 + 3} e_A^n\,. \tag{4.16}$$

5 Two-Dimensional KFVS Scheme

Here we want to solve the two-dimensional moment system

$$\frac{\partial W}{\partial t} + \frac{\partial F(W)}{\partial x} + \frac{\partial G(W)}{\partial y} = S(W)\,, \tag{5.1}$$

where

$$W = \begin{pmatrix} e \\ Q^1 \\ Q^2 \end{pmatrix}\,, \quad F(W) = \begin{pmatrix} Q^1 \\ c^2 N^{11} \\ c^2 N^{21} \end{pmatrix}\,, \quad G(W) = \begin{pmatrix} Q^2 \\ c^2 N^{12} \\ c^2 N^{22} \end{pmatrix}\,, \quad S(W) = -\frac{1}{\tau_R}\begin{pmatrix} 0 \\ Q^1 \\ Q^2 \end{pmatrix}\,.$$

We start again with a piecewise constant initial data of the conservative variables $\overline{W}^n_{i,j}$. The integration of (5.1) over thecontrol volume $[t_n, t_{n+1}] \times [x_{i-\frac{1}{2}}, x_{i+\frac{1}{2}}] \times [y_{j-\frac{1}{2}}, y_{j+\frac{1}{2}}]$ gives

$$\overline{W}^{n+1}_{i,j} = \overline{W}^n_{i,j} - \lambda \left[F^n_{i+\frac{1}{2},j} - F^n_{i-\frac{1}{2},j} \right] - \mu \left[G^n_{i,j+\frac{1}{2}} - G^n_{i,j-\frac{1}{2}} \right] + \Delta t S^n_{i,j} \,, \tag{5.2}$$

where $\lambda = \frac{\Delta t}{\Delta x}$, $\mu = \frac{\Delta t}{\Delta y}$ and

$$F^n_{i+\frac{1}{2},j} = \frac{1}{\Delta t} \int_{t_n}^{t_{n+1}} F(\tau, x_{i+\frac{1}{2}}, y_j)\, d\tau \,, \quad G^n_{i,j+\frac{1}{2}} = \frac{1}{\Delta t} \int_{t_n}^{t_{n+1}} G(\tau, x_i, y_{j+\frac{1}{2}})\, d\tau \,,$$

where the flux moments $F(\tau, x_{i+\frac{1}{2}}, y_j)$ and $G(\tau, x_i, y_{j+\frac{1}{2}})$ are given in (3.13).

If the CFL condition $\Delta t \leq \frac{1}{2} min(\Delta x, \Delta y)$ is satisfied, then we can utilize the kinetic flux vector splitting (KFVS). Since after flux splitting the fields e, Q^1 and Q^2 in (3.12) and (3.13) are not depending on the integration variables ξ and φ, therefore we can solve analytically these moments integrals for the fluxes. This gives

$$F^n_{i+\frac{1}{2},j} = F^+_{i,j} + F^-_{i+1,j} \,, \qquad G^n_{i,j+\frac{1}{2}} = G^+_{i,j} + F^-_{i,j+1} \,, \tag{5.3}$$

where

$$F^{\pm}_{i,j} = \begin{pmatrix} Q^1 \\ c^2 N^{11} \\ c^2 N^{21} \end{pmatrix}^{\pm}_{i,j}, \quad G^{\pm}_{i,j} = \begin{pmatrix} Q^2 \\ c^2 N^{12} \\ c^2 N^{22} \end{pmatrix}^{\pm}_{i,j}, \tag{5.4}$$

and (3.13) implies that

$$\begin{aligned}
(Q^1_i)^{\pm} =& 2048 Q^1_i c^2 e_i \alpha \pm \frac{256 c^2 e_i \alpha}{F_i \beta_2^3} \left(3\beta_2^4 + 6F_i^2 (Q^1_i)^2 \beta_2^2 - F_i^4 (Q^1_i)^4 \right) \,, \\
(Q^2_i)^{\pm} =& 2048 Q^2_i c^2 e_i \alpha \pm \frac{256 c^2 e_i \alpha}{F_i \beta_1^3} \left(3\beta_1^4 + 6F_i^2 (Q^2_i)^2 \beta_1^2 - F_i^4 (Q^2_i)^4 \right) \,, \\
(N^{11}_i)^{\pm} =& \pm \frac{128 \alpha Q^1_i}{\beta_2} \left(3\beta_2^2 + F_i^2 (Q^1_i)^2 \right) + \frac{128\alpha}{F_i} \left(\beta_2^2 + 3F_i^2 (Q^1_i)^2 \right) \,, \\
(N^{22}_i)^{\pm} =& \pm \frac{128 \alpha Q^2_i}{\beta_1} \left(3\beta_1^2 + F_i^2 (Q^2_i)^2 \right) + \frac{128\alpha}{F_i} \left(\beta_1^2 + 3F_i^2 (Q^2_i)^2 \right) \,, \\
(N^{21}_i)^{\pm} =& 512 \alpha F_i Q^1_i Q^2_i \pm \frac{64 Q^2_i \alpha}{\beta_2^3} \left(3\beta_2^4 + 6F_i^2 (Q^1_i)^2 \beta_2^2 - F_i^4 (Q^1_i)^4 \right) \,, \\
(N^{12}_i)^{\pm} =& 512 \alpha F_i Q^1_i Q^2_i \pm \frac{64 Q^1_i \alpha}{\beta_2^3} \left(3\beta_1^4 + 6F_i^2 (Q^2_i)^2 \beta_1^2 - F_i^4 (Q^2_i)^4 \right) \,,
\end{aligned} \tag{5.5}$$

with

$$\alpha = \frac{c^4 e_i^5 (-4 + F_i)^3}{\left[-16 c^2 e_i^2 + F_i^2 ((Q^1_i)^2 + (Q^2_i)^2) \right]^3}, \quad \beta_k = \sqrt{16 c^2 e^2 - (F^2 Q^k)^2}, \; k = 1, 2 \,. \tag{5.6}$$

Here for the fluxes $F^{\pm}_{i,j}$, we split the integrals with respect to variable ξ and take the integration with respect to variable φ as a whole. While for the fluxes $G^{\pm}_{i,j}$, we split the integrals with respect to variable φ and integrate the integrals with respect to ξ as a whole. Thus we have the following conservative scheme

$$\begin{aligned}\overline{W}^{n+1}_{i,j} = \overline{W}^{n}_{i,j} &- \lambda\left[F^{+}_{i} + F^{-}_{i+1,j} - F^{+}_{i-1,j} - F^{-}_{i,j}\right] \\ &- \mu\left[G^{+}_{i,j} + G^{-}_{i,j+1} - G^{+}_{i,j-1} - G^{-}_{i,j}\right] + \Delta t S^{n}_{i,j}\,. \end{aligned} \tag{5.7}$$

5.1 Second Order Extension of the Scheme in 2D

Here we present the second-order MUSCL-type approach for the two-dimensional case. Keeping in view the MUSCL approach discussed in the previous section for the one-dimensional case, we have again the following three steps.

(I): **Data Reconstruction and Boundary Extrapolated Values.** Starting with a piecewise-constant solution in time and space, $\overline{W}^{n}_{i,j}$, one reconstruct a piecewise linear (MUSCL-type) approximation independently in x- and y-directions by selecting respective slope vectors (differences) W^{x} and W^{y}. Boundary extrapolated values are

$$\begin{aligned} W^{LX}_{i,j} &= \overline{W}^{n}_{i,j} - \frac{1}{2}W^{x}_{i,j}\,, \quad W^{RX}_{i,j} = \overline{W}^{n}_{i,j} + \frac{1}{2}W^{x}_{i,j}\,, \\ W^{LY}_{i,j} &= \overline{W}^{n}_{i,j} - \frac{1}{2}W^{y}_{i,j}\,, \quad W^{RY}_{i,j} = \overline{W}^{n}_{i,j} + \frac{1}{2}W^{y}_{i,j}\,. \end{aligned} \tag{5.8}$$

A possible computation of these slopes, is given by family of *discrete derivatives* parameterized with $1 \le \theta \le 2$, for example

$$\begin{aligned} W^{x}_{i,j} &= MM\left\{\theta\Delta\overline{W}_{i+\frac{1}{2},j}, \frac{\theta}{2}\left(\Delta\overline{W}_{i+\frac{1}{2},j} + \Delta\overline{W}_{i-\frac{1}{2},j}\right), \theta\Delta\overline{W}_{i-\frac{1}{2},j}\right\}\,, \\ W^{y}_{i,j} &= MM\left\{\theta\Delta\overline{W}_{i,j+\frac{1}{2}}, \frac{\theta}{2}\left(\Delta\overline{W}_{i,j+\frac{1}{2}} + \Delta\overline{W}_{i,j-\frac{1}{2}}\right), \theta\Delta\overline{W}_{i,j-\frac{1}{2}}\right\}\,. \end{aligned}$$

Here Δ denotes central differencing,

$$\Delta\overline{W}_{i+\frac{1}{2},j} = \overline{W}_{i+1,j} - \overline{W}_{i,j}, \qquad \Delta\overline{W}_{i,j+\frac{1}{2}} = \overline{W}_{i,j+1} - \overline{W}_{i,j}\,,$$

and MM denotes the min-mod nonlinear limiter given by (4.10).

(II): **Evolution of Boundary Extrapolated Values.** The boundary extrapolated values are evolved at a time $\frac{\Delta t}{2}$ by using

$$\hat{W}^{l}_{i,j} = W^{l}_{i,j} + \lambda\left[F(W^{LX}_{i,j}) - F(W^{RX}_{i,j})\right] + \mu\left[G(W^{LY}_{i,j}) - G(W^{RY}_{i,j})\right] + \frac{\Delta t}{2}\overline{S}^{n}_{m,i}\,, \tag{5.9}$$

for $l = LX, RX, LY, RY$. Further, to calculate the source term at half time step, we need

$$\overline{W}^{n+\frac{1}{2}}_{i,j} = \overline{W}^{n}_{i,j} - \lambda\left[F(W^{n}_{i+1,j}) - F(W^{n}_{i,j})\right] - \mu\left[G(W^{n}_{i,j+1}) - G(W^{n}_{i,j})\right] + \frac{\Delta t}{2}\overline{S}^{n}_{m,i}\,. \tag{5.10}$$

(III): **Solution at the Next Time Step.** At each intercell position one solves

$$\overline{W}_{i,j}^{n+1} = \overline{W}_{i,j}^{n} - \lambda \left[F_{i+\frac{1}{2},j}^{n+\frac{1}{2}} - F_{i+\frac{1}{2},j}^{n+\frac{1}{2}} \right] - \mu \left[G_{i,j+\frac{1}{2}}^{n+\frac{1}{2}} - G_{i,j+\frac{1}{2}}^{n+\frac{1}{2}} \right] + \Delta t S_i^{n+\frac{1}{2}} , \qquad (5.11)$$

where

$$F_{i+\frac{1}{2},j}^{n+\frac{1}{2}} = F^{+}(\hat{w}_{i,j}^{RX}) + F^{-}(\hat{w}_{i+1,j}^{LX}) , \;\; G_{i,j+\frac{1}{2}}^{n+\frac{1}{2}} = G^{+}(\hat{w}_{i,j}^{RY}) + G^{-}(\hat{w}_{i,j+1}^{LY}) .$$

6 Numerical Examples

In order to validate our results obtained in the previous sections, we present some numerical test cases. We consider the numerical test cases for the one and two-dimensional cases. For the comparison of the results we use high order central schemes [6, 11, 12].

6.1 Two Interacting Heat Pulses

This one-dimensional test problem demonstrates the interaction of two heat pulses, which leads to a large increase of the energy density at the collision point during a short time interval. The initial data are

$$e(0,x) = \begin{cases} 1 , & x \le 0.3 \\ 2 , & 0.3 \le x \le 0.4 \\ 1 , & 0.4 \le x \le 0.6 \\ 2 , & 0.6 \le x \le 0.7 \\ 1 , & x \le 1.0 \end{cases} , \quad Q(0,x) = \begin{cases} 0 , & x \le 0.3 \\ 1 , & 0.3 \le x \le 0.4 \\ 0 , & 0.4 \le x \le 0.6 \\ -1 , & 0.6 \le x \le 0.7 \\ 0 , & x \le 1.0 \end{cases} . \qquad (6.1)$$

We solve the moment system for the above problem at time $t = 0.5$ for $\tau_R = 1.0$. We take 200 mesh points in the $x-$space. Figure 3 shows the results. From the comparison of the initial and final curves of energy density, we observe a large increase of the energy density e at the collision point $x = 0.5$.

6.2 Reflection of a Single Shock

Here consider a single shock solution for the moment system with reflecting boundary conditions at the lower boundary $x = 0$. The initial data are

$$(e,Q)(0,x) = \begin{cases} (1,0) , & x \le 0.5 , \\ \left(2, -\frac{1}{\sqrt{3}} \sqrt{\frac{3\sqrt{2}-1}{\sqrt{2}+1}}\right) , & x \ge 0.5 . \end{cases} \qquad (6.2)$$

This single shock data was obtained in [4] by using Rankine-Hugoniot jump conditions. The computational domain is $0 \le x \le 1$. Here we take 200 mesh points in $x-$space. Figure 4 show the results. The first row in Figure 4 show the results from second order KFVS scheme in the time range $0 \le t \le 1.7$, while the last two rows are the comparison of the results from KFVS and central schemes at time $t = 1.7$.

6.3 Periodic Boundary Conditions

In the following one-diemsional numerical problem we apply the inflow boundary conditions to the moment system. We observe the following phenomena:

a) the formation and steeping of shock fronts,
b) the speed of shock front is apparently larger than $\frac{c}{\sqrt{3}}$,
c) the broadening of initial heat pulses at later times.

Here we create a periodic heat pulse

$$e_w(t) = 2 - \cos(8\pi t)\,, \tag{6.3}$$

at the lower boundary. The initial data are $e_0 = 1$ and $Q_0 = 0$, and the computational doamin is $0 \leq x \leq 1.5$. Here $e_w(t)$ is prescribed but $Q_w(t)$ is calculated according to (4.15) and (4.16). Surprisingly in this case $Q_w(t)$ meet the value which can be obtained by shock conditions in [4]. Figure 5 gives the results. The first row in Figure 5 show the boundary data, while the second and third rows illustrate the solutions at $t = 1.5$. The formation and steepening of shock fronts is clearly visible. We take 200 mesh points in the spatial domain.

6.4 Heat Pulse in 2D

In this example we consider a two-dimensional energy pulse inside a square box of sides length 0.02, with out-flow boundaries. Initially the heat fluxes are zero. The energy density is 1.5 inside a small square box of sides length 0.02 in the center of the large box, while energy density is unity elsewhere. The results are shown at $t = 1.2$ in Figures 6. In all the results we have used 200×200 mesh points. We take $\tau_R = \infty$.

6.5 Explosion in a Box.

In this example we consider a two-dimensional energy pulse inside a square box of sides length 2.0, with periodic boundaries. Initially the heat fluxes are zero. The energy density is 2.0 inside a small square box of sides length 0.5 in the center of the large box, while energy density is unity elsewhere. The results are shown in Figures 7 at $t = 0.5$, $t = 1.5$ and $t = 2.0$. In all the results we have used 300×300 mesh points. We take $\tau_R = \infty$.

6.6 Inflow IBVP in 2D

This problem represent the propagation of heat pulse

$$e_w(t) = \begin{cases} 1\,, & t \leq 0.0\,, \\ 3\,, & 0.0 < t \leq 0.5\,, \\ 1\,, & t > 0.5\,, \end{cases} \tag{6.4}$$

which is generated at lower xy-boundaries. The initial data are $e_0 = 1$ and $Q_0^1 = 0$, $Q_0^2 = 0$, and the computational domain is $0 \leq x, y \leq 1.5$. Note that only $e_w(t)$ is prescribed, while $Q_w^1(t)$ and $Q_w^2(t)$ are calculated numerically form this data. Figure 8 gives the results. The first and second rows in Figure 8 illustrate the solution at time $t = 1.5$ and $y = 1$. The third row give the surface plots of the energy density and heat flux Q^1 at $t = 1.5$. We have used 200×200 mesh points.

7 Conclusions

In this paper we have derived first- and second-order KFVS schemes for the solution of initial and boundary value problems (IBVP) for the hyperbolic heat conduction equations. We have numerically implement these schemes in one and two space dimensions. The fluxes in the KFVS schemes where calculated by using flux-vector splitting technique on the free flight flux moment integrals at the cell interface. The reduction of the three-dimentional moment intgerals to surface integrals and their further reduction in one- and two-dimensional cases enable us to integrate analytically the flux splitted integrals by using Matlab or Maple packages. We have extend the scheme to account for the boundary conditions by using a continuity condition. The application of the boundary conditions in KFVS schemes are exactly the same as in Godunov upwind schemes. For the comparison of the results we have used central schemes. Similar to central schemes, the programing code for the KFVS schemes are compact and simpler. It was found that KFVS schemes have better resultion from the central schemes.

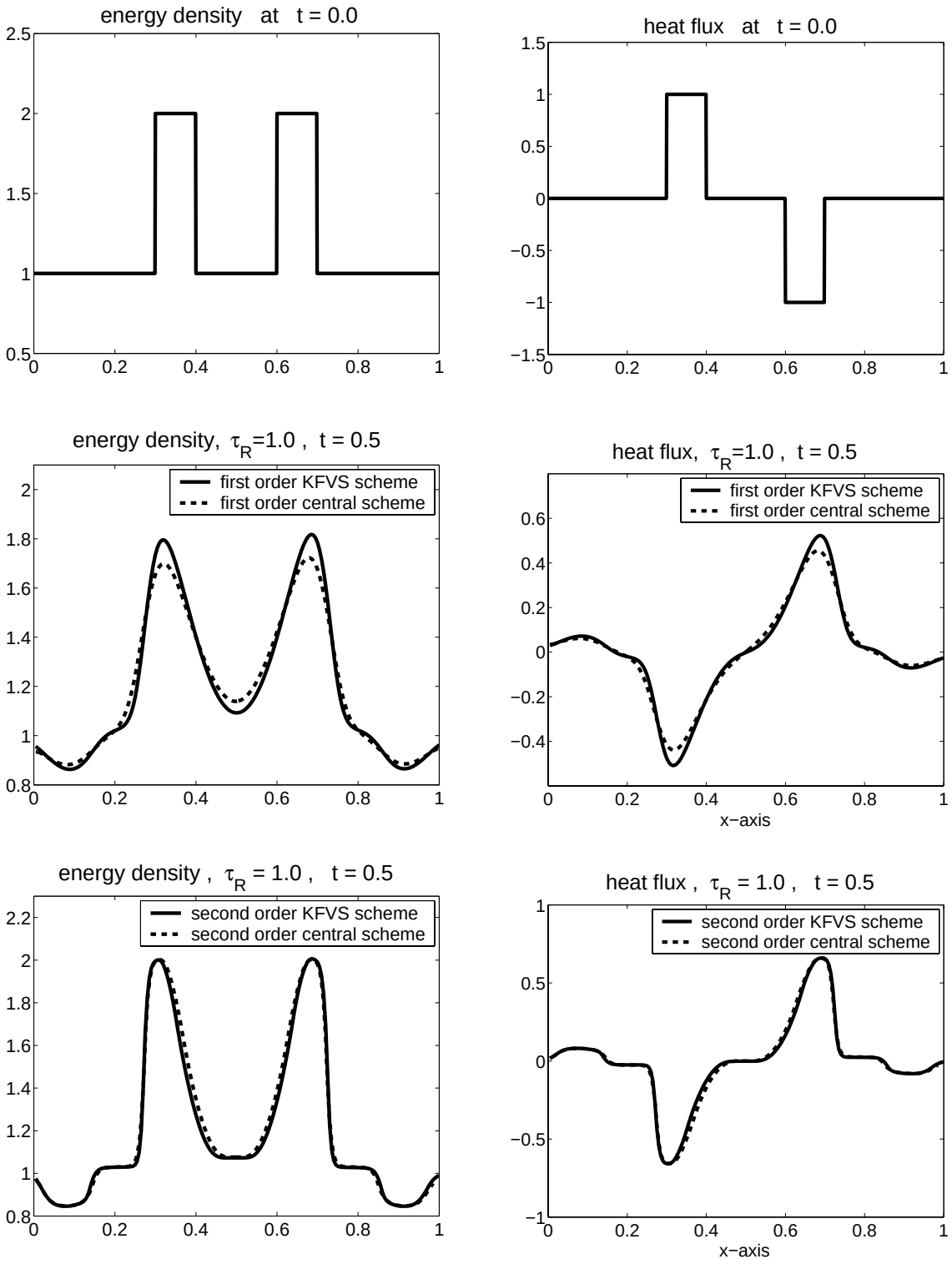

Figure 3: Interaction of two pulses.

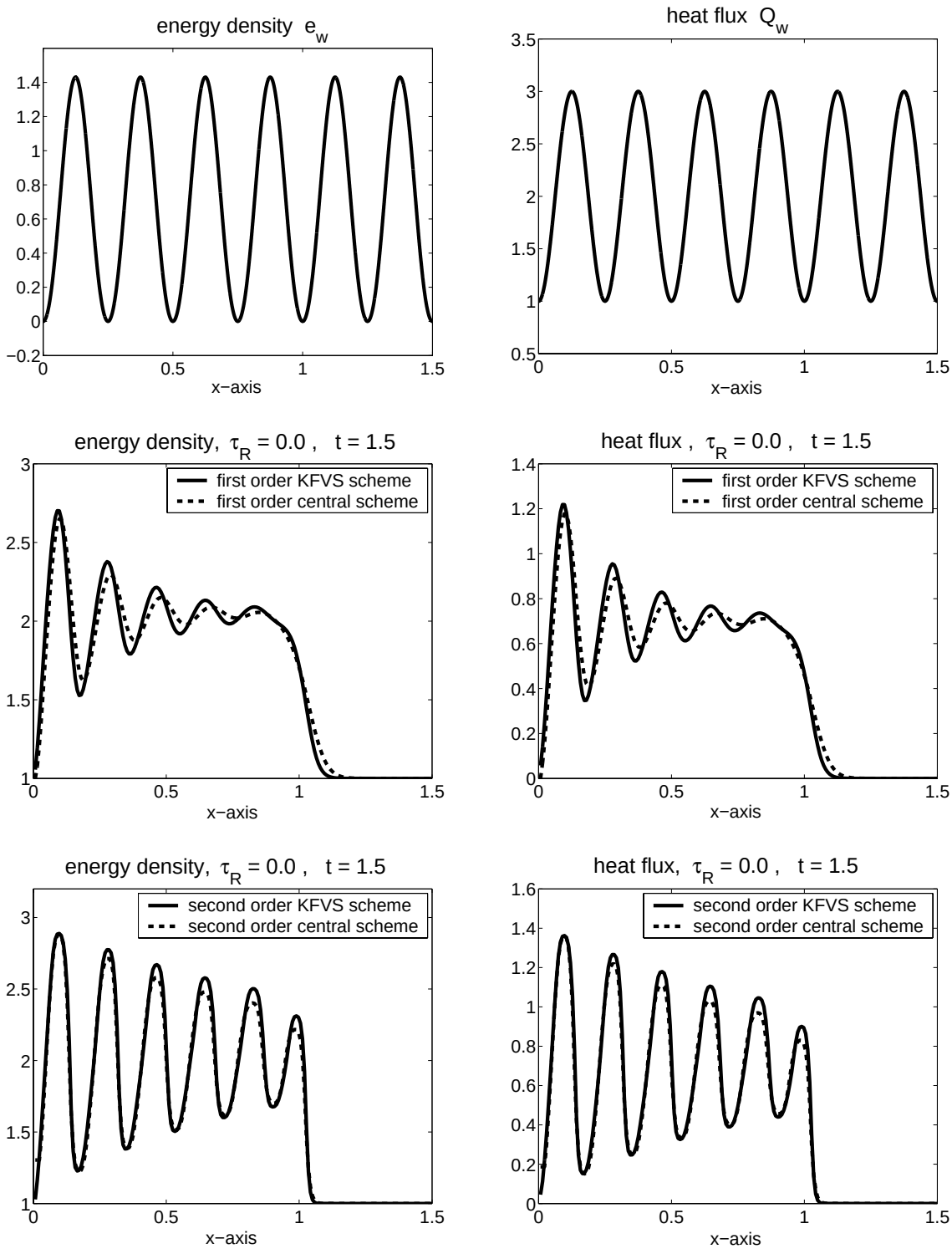

Figure 4: Periodic boundary conditions

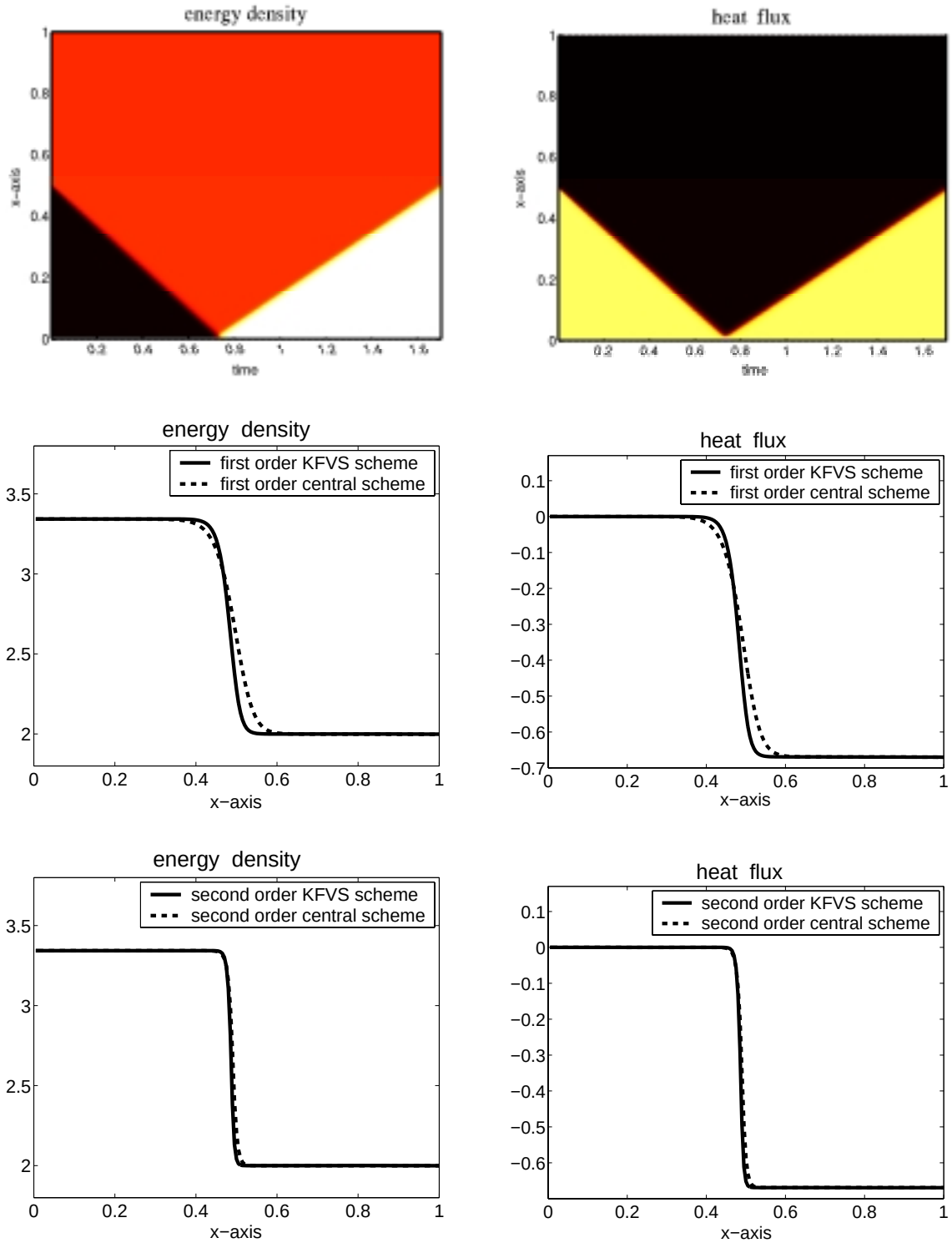

Figure 5: A single shock reflection

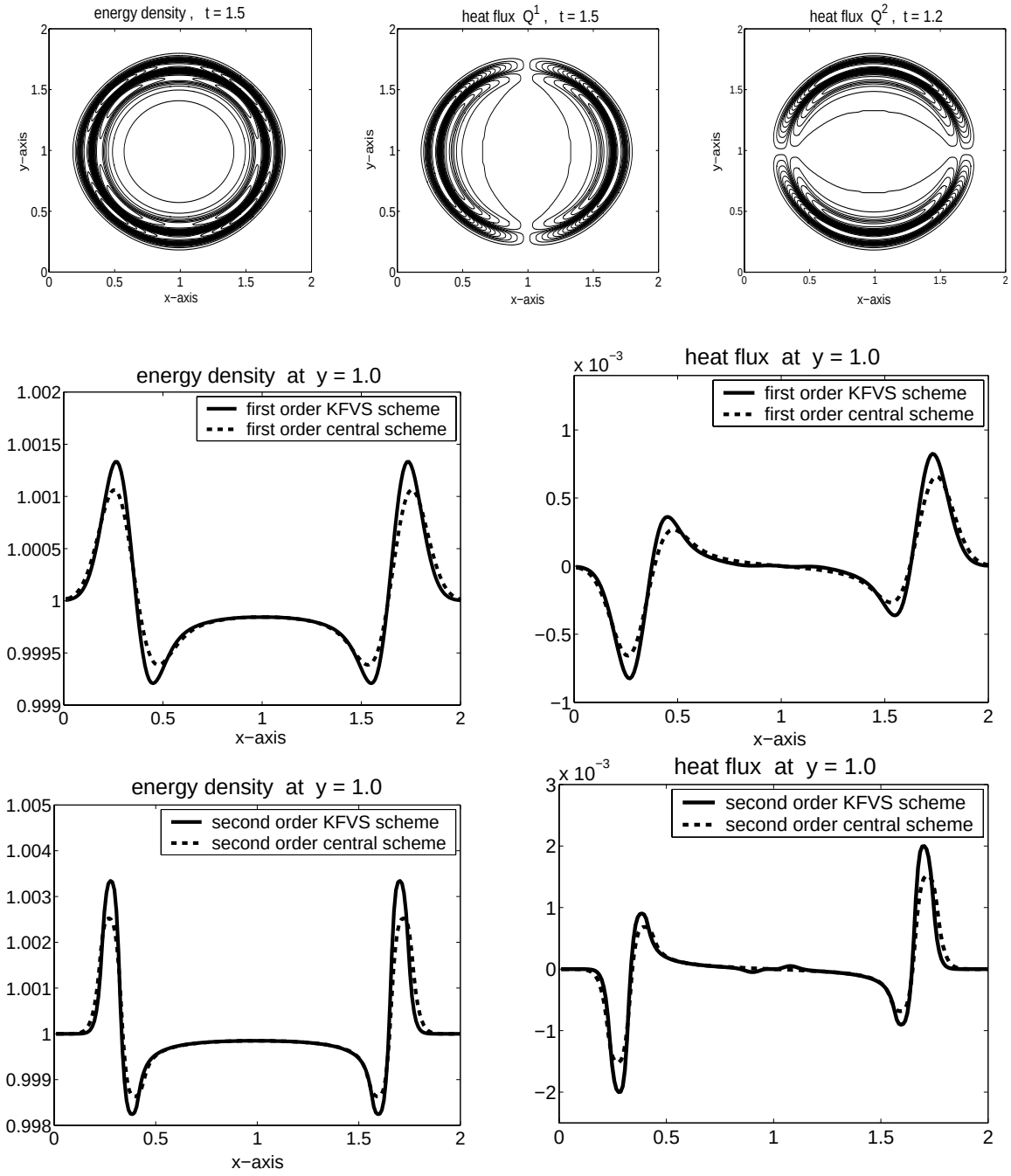

Figure 6: Evolution of energy density and heat flux in 2D.

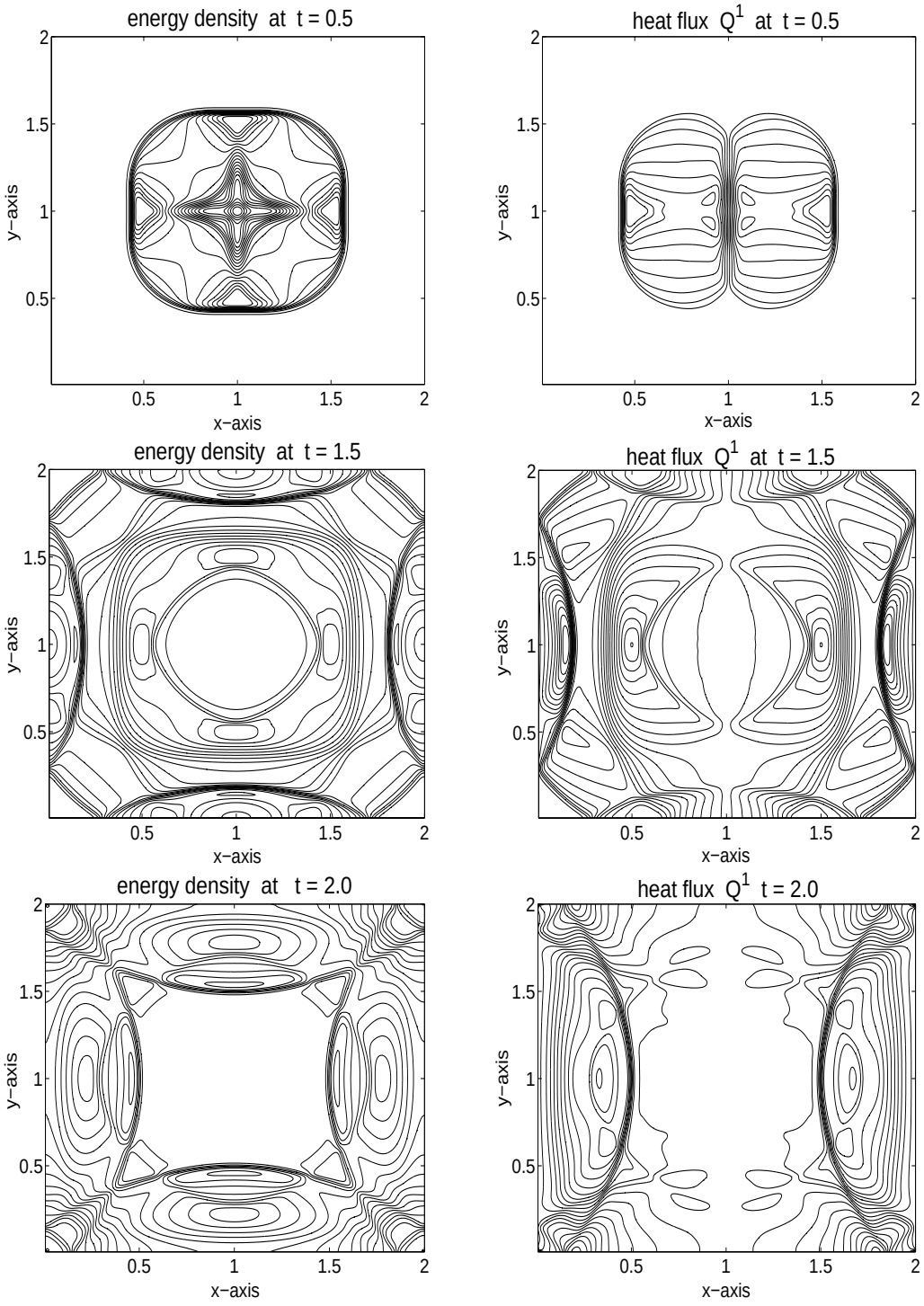

Figure 7: Explosion in a box problem.

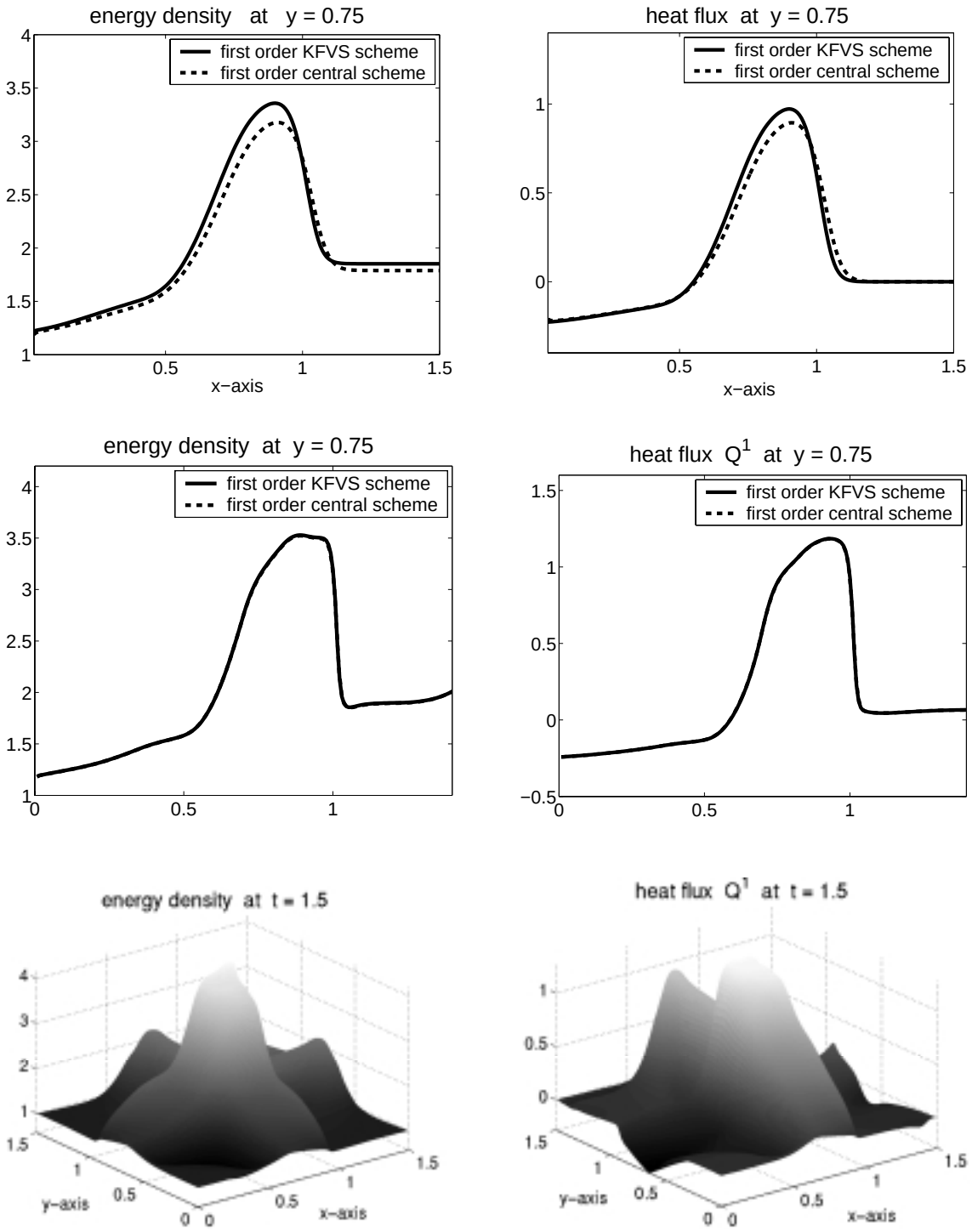

Figure 8: Inflow initial and boundary value problem.

References

[1] J. Callaway, "Quantum theory of the solid state", Academic press, San Diego, 1991.

[2] W. Dreyer and M. Kunik, "Initial and boundary value problems of hyperbolic heat conduction", *Cont. Mech. Thermodyn.* **11.4** (1999) pp. 227-245.

[3] W. Dreyer, M. Herrmann and M. Kunik, "Kinetic solutions of the Boltzmann-Peierls equation and its moment systems", *WIAS-Preprint* No. **709**, Berlin (2001).

[4] W. Dreyer, S. Seelecke, "Entropy and causality as criteria for the existence of shock waves in low temperature heat conduction", *Cont. Mech. Thermodyn.,* **4**, (1992) pp. 23-36.

[5] W. Dreyer, H. Struchtrup, "Heat pulse experiments revisited", *Cont. Mech. Thermodyn.,* **5**, (1993) pp. 1-50.

[6] G.-S. Jaing , E. Tadmor, "non-oscillatory central schemes for multidimensional hyperbolic conservation laws", *SIAM J. Sci. Comput.* **19**, (1998), pp. 1892-1917.

[7] M. Kunik, S. Qamar and G. Warnecke, "Kinetic schemes for the ultra-relativistic Euler equations", *J. Comput. Phys.* **187**, (2003), pp. 572-596.

[8] M. Kunik, S. Qamar and G. Warnecke, "A BGK-type kinetic flux-vector splitting schemes for the ultra-relativistic relativistic gas dynamics", Preprint Nr. **4**, Otto-von-Guericke University, (2003).

[9] M. Kunik, S. Qamar and G. Warnecke, "A reduction of the Boltzmann-Peierls equation", Preprint Nr. **6**, Otto-von-Guericke University, (2003).

[10] M. Kunik, S. Qamar and G. Warnecke, "Second order accurate kinetic schemes for the ultra-relativistic Euler equations", Preprint Nr. **18**, Otto-von-Guericke University, (2003).

[11] S.F. Liotta, V.R. Romano and G. Russo, "Central schemes for balance laws of relaxation type", *SIAM J. Numer. Anal.* 38 (2000), pp. 1337-1356.

[12] H. Nessayahu, E. Tadmor, "Non-oscillatory central differencing fo hyperbolic conservation Laws",*SIAM J. Comput. Phys.* **87**, (1990), pp. 408-448.

[13] R.E. Peierls, "Quantum theory of solids", Oxford University press, London 1995.

[14] E.F. Toro, "Riemann solvers and numerical method for fluid dynamics", Second Edition, Springer-Verlag, (1999).

[15] K. Xu, "Gas evolution dynamics in Godunov-type schemes and analysis of numerical shock instability", ICASE Report No. Tr. 99-6, (1998).